diffraction fringes in the diffracted or forward-scattering beams (26). Such experiments are realizable, probably using an Authier collimator and synchrotron-radiation impulses. A high-quality homogeneous AW is necessary for the success of such experiments.

We used boundary conditions (3). What can we expect when $T = (2n+1)\lambda_s/2$, $n = 1, 2, \ldots$? The suppression μ_s will not be as strong as before because this value is defined by the probability of scattering at the layer thickness $\lambda_s/2$, $P \simeq q^2$ [(15)] instead of $P \simeq q^4$ [(19)].

What can we say about μ_s dependence on the AW frequency? We have found $\mathbf{W}_0$ [(15)] using direct numerical solution of the Takagi–Taupin equations for the layer thickness $\lambda_s/2$ and momentum $q = 0$. The results of the numerical solution of the TT equations with AW amplitude $\mathbf{W} = \mathbf{W}_0$ and thickness of crystal $T = 500\,\mu\text{m}$ are presented in Fig. 6. Low-frequency AWs lead to a small suppression of the diffracted beam (Fig. 6*a*). Strong suppression of the diffracted beam is realized for the case of high-frequency ultrasound ($k_s \gg \Delta k_0$) when $J_0(4\mathbf{HW}) \simeq 0$, that is $\mathbf{HW} \simeq 0.6003$, $1.375, \ldots$ (J_0 is the Bessel function). High-frequency AWs strongly increase μ_s for our schematic model ($\tau = 115$, $T = 500\,\mu\text{m}$) with suppression of the diffracted-beam intensity; $\mu_s \simeq 5 \times 10^4$ (!) when $\lambda_s = 10\,\mu\text{m}$. The smoothing curve of the intensity of the diffracted beam (Fig. 6*b*) is well approximated as

$$I_h \simeq 2.8 \times 10^{-5}(\delta\Theta/\Delta\Theta_0)^{2.2} \qquad (28)$$

when $|\delta\Theta/\Delta\Theta_0| < 3$. Therefore, high-frequency ultrasonic AWs ($\lambda_s = 10\,\mu\text{m}$) and probably hypersound also lead to the strong and rapid suppression of the intensity of the diffracted beam outside the center of the diffraction pattern. This effect can be explained by the coefficients $C \simeq 1/k_s^{2-3}$ (18) when $\lambda_s < \tau$. Therefore, suppression of μ_s is large and exists in a wide angular interval of the incident beam. The crystal ($T = 500\,\mu\text{m}$) is effectively divided into many thin layers ($\lambda_s = 10\,\mu\text{m}$). The amplitude of scattering is very small in each of these thin layers.

It is likely that the rapid and deep suppression and oscillation of the intensity of the diffracted beam induced by ultrasound or hypersound could be used, in principle, for shielding electronic apparatus from the short powerful impulses of highly collimated monochromatic SR beams. The shielding from SR impulses is discussed in experiments with SR excitation of Mössbauer nuclei.

A considerable part of this work was done during the author's visit to the Nuclear Physics Institute (Rez, near Prague). I wish to express my appreciation to Professor P. Mikula, Dr P. Lukas and their colleagues for the hospitality. I am most grateful to Dr M. Vrana for many interesting discussions and to Dr L. Sedlakova, J. Saroun, P. Strunz, B. Michalkova and J. Vavra for their great technical assistance. I am especially grateful to L. Rusevich and Dr A. Muromtsev for the creation of the computer program.

References

ENTIN, I. R. (1977). *Pis'ma Zh. Eksp. Teor. Fiz.* **26**, 392–395.
ENTIN, I. R. & PUCHKOVA, I. A. (1984). *Fiz. Tverd. Tela*, **26**, 3320–3324.
IOLIN, E. M. & ENTIN, I. R. (1983). *Zh. Eksp. Teor. Fiz.* **86**, 1692–1700.
IOLIN, E. M., RAITMAN, E. A., KUVALDIN, B. V. & ZOLOTOYABKO, E. V. (1988). *Zh. Eksp. Teor. Fiz.* **94**, 218–233.
IOLIN, E. M., ZOLOTOYABKO, E. V., RAITMAN, E. A., KUVALDIN, B. V. & GAVRILOV, V. N. (1986). *Zh. Eksp. Teor. Fiz.* **91**, 2132–2139.
KÖHLER, R., MÖHLING, W. & PEIBST, H. (1974). *Phys. Status Solidi B*, **61**, 173–180, 439–447.
KULDA, J., VRANA, M. & MUKULA, P. (1988). *Physica (Utrecht)*, B**151**, 122–129.
LANDAU, L. D. & LIFSHITZ, E. M. (1965). *Quatum Mechanics*. Oxford: Pergamon.
LUKAS, P. & KULDA, J. (1989). *Phys. Status Solidi B*, **6**, 41–48.
MIKULA, P., LUKAS, P. & KULDA, J. (1992). *Acta Cryst.* A**48**, 72–73.
SPENCER, W. J. & PEARMAN, G. T. (1970). *Adv. X-ray Anal.* **13**, 507–527.

Acta Cryst. (1995). A**51**, 902–909

A Basic Factor of Dual Epitaxy: the Symmetry of Similarity of Zinc Blende Structure

BY LIN LI

North China Research Institute of Electro-optics, Beijing 100015, *People's Republic of China*

(*Received* 7 *November* 1994; *accepted* 19 *June* 1995)

Abstract

The symmetry of the similarity of the surface step structure in zinc blende (sphalerite) type structures is investigated by studying the crystal planes that are parallel to the $[01\bar{1}]$ axis. The symmetry transformations of the similar plane pairs are derived. Plane sets (111) and (311) are the planes of symmetry. The similarity of the surface step structure exists among three sets of planes. The surface geometric characteristics of similar

planes are discussed. The result can be applied to explain dual epitaxy and optimize the interface quality by designing dual epitaxy in the heteroepitaxy.

1. Introduction

It has been found that the growth of CdTe on (100), (211) and (311) GaAs by molecular-beam epitaxy or metal-organic vapor-phase epitaxy can result in dual epitaxy, *i.e.* the occurrence of (100) or (111) CdTe on (100) GaAs (Nishitani, Ohkata & Murotani, 1983), (211) or (133) CdTe on (211) GaAs (Lange *et al.*, 1991) and (011) or (311) CdTe on (311) GaAs (Smith, Byrne, Patel, Knowles & Thompson, 1990).

The occurrence of dual epitaxy depends on many factors, such as the surface reconstruction, which is related to the preparation of the substrate surface (Otsuka *et al.*, 1985; Ponce, Anderson & Ballingall, 1986; Cohen-Solar, Bailly & Barbe, 1986; Feldman & Austin, 1986; Ortner & Bauer, 1988), the twin operation (Cinader & Raizman, 1992), the stacking sequence of the wurtzite-type structure on the GaAs surface (Nakamura, Otsuka, Lange, Sporker & Faurie, 1992) and kinetics, which relates to the substrate temperature.

In this paper, we focus on the geometric symmetry of similarity of the zinc blende structure and then use the conclusion to explain the three kinds of dual epitaxy mentioned above and to design new dual epitaxy for reducing interfacial mismatch.

2. The symmetry of similarity of the surface step structure

Fig. 1 is the projection of the zinc blende structure in the [011] direction. Each lattice point with Miller indices denotes a crystal plane that goes through the origin and this lattice point. The distance from this lattice point to the origin is the periodic unit length of the projection of this crystal plane, which is given by

$$D(hka) = \tfrac{1}{2}(\tfrac{1}{2}h^2 + k^2)^{1/2}a, \qquad (1)$$

where a is the lattice constant.

In this paper, for convenience and because we are only interested in the surface structure of crystal planes, let any set of planes be represented by the lowest group of Miller indices h, k ($l = k$) that satisfies $h + k =$ even. For instance, (100), (200), (300), ... are represented by (200); (011), (022), (033), ... by (022); (111), (222), (333), ... by (111); (211), (422), (633), ... by (422).

It is seen in Fig. 1, on both sides of the (111) or (311) plane, that there are two series of paired planes. The two crystal planes of each pair have a similar surface step structure within every unit length and are symmetrical about (111) or (311). For example, (133)/(422), (022)/(311) and (244)/(533) plane pairs are symmetrical about (111) but (111)/(200), (422)/(511) and (533)/(711) plane pairs are symmetrical about (311). The surface step structures of these planes are shown in Fig. 2.

Let $(h_1k_1k_1)/(h_2k_2k_2)$ be a pair of crystal planes that have similar surface step structure and are symmetrical

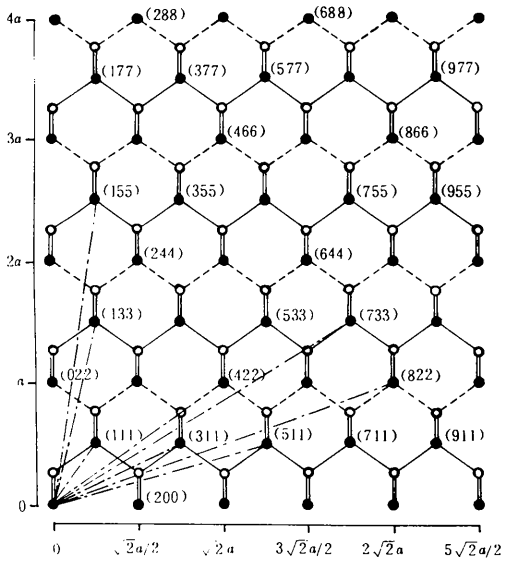

Fig. 1. The projection of the zinc-blende-structure crystal in the [01$\bar{1}$] orientation. Each lattice point with Miller indices denotes a crystal plane that goes through the origin and this lattice point (some of them are marked with dashed-dotted lines). The spacing between the planes of single-line-represented bonds and dashed-line-represented bonds is $(2^{1/2}/4)a$.

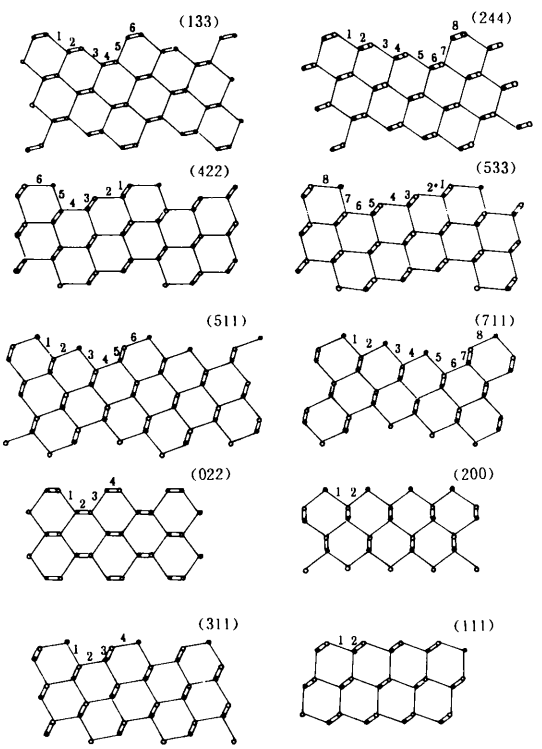

Fig. 2. The surface steps of some planes.

about plane (111), then the two planes must satisfy the following transformation relation:

$$\begin{pmatrix} h_1 \\ k_1 \end{pmatrix} = \tfrac{1}{2}\begin{pmatrix} -1 & 3 \\ 1 & 1 \end{pmatrix}\begin{pmatrix} h_2 \\ k_2 \end{pmatrix}, \qquad \begin{pmatrix} h_2 \\ k_2 \end{pmatrix} = \tfrac{1}{2}\begin{pmatrix} -1 & 3 \\ 1 & 1 \end{pmatrix}\begin{pmatrix} h_1 \\ k_1 \end{pmatrix}. \tag{2}$$

This is a reversible transformation.

For a pair of planes that have similar surface step structure and are symmetrical about plane (311), there is a transformation relation:

$$\begin{pmatrix} h_1 \\ k_1 \end{pmatrix} = \tfrac{1}{2}\begin{pmatrix} 1 & 3 \\ 1 & -1 \end{pmatrix}\begin{pmatrix} h_2 \\ k_2 \end{pmatrix}, \qquad \begin{pmatrix} h_2 \\ k_2 \end{pmatrix} = \tfrac{1}{2}\begin{pmatrix} 1 & 3 \\ 1 & -1 \end{pmatrix}\begin{pmatrix} h_1 \\ k_1 \end{pmatrix}. \tag{3}$$

It is also a reversible transformation.

The reversibility of both the transformations suggests that the symmetry about planes (111) and (311) is true. It is an 'oblique' symmetry, in which plane (311) reflects points along $(1\bar{1}\bar{1})$ and plane $(1\bar{1}\bar{1})$ reflects points along (311). In Figs. 4 and 5, this character is clearly visible.

Making a more detailed examination of the direction of the steps and the polarity of dangling bonds on the surface, we modify the similarity transformation relations into the following form:

equation (2) to

$$\begin{pmatrix} h_1 \\ k_1 \end{pmatrix} = \tfrac{1}{2}\begin{pmatrix} -1 & -3 \\ 1 & -1 \end{pmatrix}\begin{pmatrix} h_2 \\ k_2 \end{pmatrix}, \qquad \begin{pmatrix} h_2 \\ k_2 \end{pmatrix} = \tfrac{1}{2}\begin{pmatrix} -1 & 3 \\ -1 & -1 \end{pmatrix}\begin{pmatrix} h_1 \\ k_1 \end{pmatrix}; \tag{4}$$

equation (3) to

$$\begin{pmatrix} h_1 \\ k_1 \end{pmatrix} = \tfrac{1}{2}\begin{pmatrix} -1 & 3 \\ -1 & -1 \end{pmatrix}\begin{pmatrix} h_2 \\ k_2 \end{pmatrix}, \qquad \begin{pmatrix} h_2 \\ k_2 \end{pmatrix} = \tfrac{1}{2}\begin{pmatrix} -1 & -3 \\ 1 & -1 \end{pmatrix}\begin{pmatrix} h_1 \\ k_1 \end{pmatrix}. \tag{5}$$

Transformation (4) is the inverse transformation of (5) and they are revolving transformations. If we start from h_1, k_1 and operate with transformation (4), we obtain the following cycle:

$$(h_1, k_1)\xrightarrow[(4)]{1\quad 2}\rightarrow[-\tfrac{1}{2}(h_1 - 3k_1), -\tfrac{1}{2}(h_1 + k_1)]$$
$$\xrightarrow[(4)]{1\quad 2}\rightarrow[-\tfrac{1}{2}(h_1 + 3k_1), \tfrac{1}{2}(h_1 - k_1)]$$
$$\xrightarrow[(4)]{1\quad 2}\rightarrow(h_1, k_1).$$

This cycle goes through three crystal planes. This means that a similarity between the surface step structures exists among the three crystal planes.

In addition, it can be demonstrated that the indices h, k of one of the three similar crystal planes are even numbers and the h, k of the other two planes are odd numbers.

But for symmetry planes (111) and (311), there are only two independent planes in each of their similar planes groups, *i.e.* (111)/(200) and (311)/(022) plane pairs.

As an example, the interfacial atomic arrangements of the group $(1\bar{3}\bar{3})$, $(\bar{5}11)$ and (422) are shown in Fig. 3.

The symmetry around (111) and (311) planes described here is not covered in the normal crystal symmetry. It can be seen in Fig. 1 that, if the unit lengths of (111) and (200) planes are equal, the symmetry around (111) and (311) planes would be the same as the symmetry around (200) and (022) planes but in fact the symmetry around (111) and (311) planes is oblique or similar.

3. The characteristics of the surface structure of similar plane pairs

A. The number of dangling bonds on the crystal surface

The numbers of dangling bond projections in the $[01\bar{1}]$ orientation (see Fig. 1) within the unit-cell length $D(hka)$ of a crystal surface, which is denoted by n_{pb}, are listed in Fig. 4. On the two sides of an atomic plane, the values of n_{pb} are usually different; both numbers for each plane are given in Fig. 4. However, if h is a multiple of four or zero, the spacings between adjacent atomic planes are

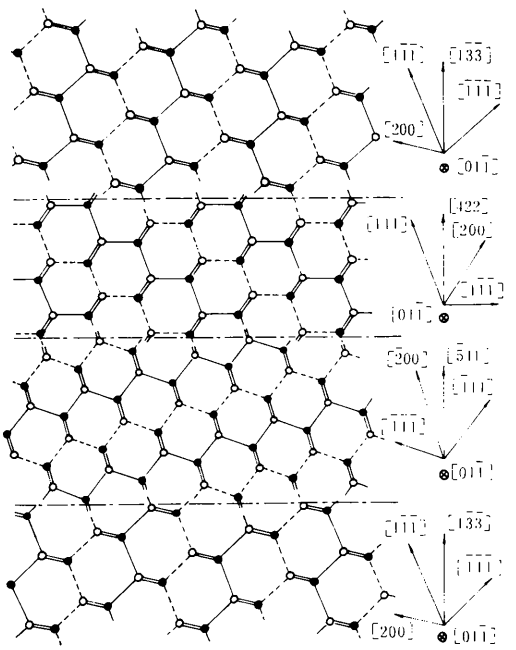

Fig. 3. The planar interfacial atomic arrangements of planes group $(1\bar{3}\bar{3})$, $(\bar{5}11)$ and (422).

even and the values of n_{pb} are the same on both sides of each atomic plane. The dashed lines in Fig. 4 indicate the positions of symmetry planes $(1\bar{1}\bar{1})$ and (311). In order to reflect the symmetry visually, the values of n_{pb} are only written for the planes for which the similar pair is also present in Fig. 4 and which are symmetrical about (311) and $(1\bar{1}\bar{1})$.

It can be seen from Fig. 4 that, for every similar plane pair, there is always a pair of surfaces with the same value of n_{pb}. This is not always true for similar plane pairs with higher Miller indices.

The numbers of dangling bonds within the unit-cell area of crystal surface $D(hka)(2^{1/2}/2)a$, which are denoted by n_b, are listed in Fig. 5. It can be seen in Fig. 5 that, for the planes located between (211) and $(2\bar{1}\bar{1})$ or the planes for which the index h is a multiple of four or zero, the values of n_b on both sides of each atomic plane are the same; for the other planes, the difference between the values of n_b on both sides of each atomic plane is two.

Comparing the values of n_b of each plane with that of its similar pair, we find that one of the values of n_b of a plane located between (311) and $(1\bar{1}\bar{1})$ or $(\bar{3}\bar{1}\bar{1})$ and $(\bar{1}11)$ is always greater than one of the values of n_b of its similar pair located between $(\bar{1}11)$ and (311) or $(1\bar{1}\bar{1})$ and $(\bar{3}\bar{1}\bar{1})$.

B. Surface charge

The net charge number of an ideal surface is determined by the product of the valency charge number and the difference between the numbers of dangling bonds of anions and cations. Let n_{nb} denote the difference between the numbers of dangling bonds of anions and cations within the surface unit-cell area $D(hka)(2^{1/2}/2)a$ (simply called 'net bond number), then we find that:

when $h = 4m$ (m is an arbitrary integer including zero), $n_{nb} = 0$, *i.e.* the surface is nonpolar;

when $h = 4m + 2$, $n_{nb} = \pm 2$;

when $h = 4m \pm 1$ (*i.e.* odd number), $n_{nb} = \pm 1$ or ± 3 for the surfaces on the two sides of an atomic plane, respectively.

Obviously, the general trend is that the higher the Miller indices h, k of the surface, *i.e.* the longer the unit length of the surface $D(hka)$, the lower the density of the surface charge, *i.e.* the weaker the polarity of the surface.

C. The ratio of the unit lengths of each pair of surfaces

Let us introduce the ratio R of the unit length of a surface $(h_2k_2k_2)$ to that of its similar pair $(h_1k_1k_1)$,

$$R = D(h_2k_2a)/D(h_1k_1a). \tag{6}$$

For simplicity, suppose the two planes are related by the transformation (3). The polar diagram of the value of R *versus* the azimuth of plane $(h_1k_1k_1)$ is plotted in Fig. 6. The radial dimension indicates the value of R. The azimuth of plane $(h_1k_1k_1)$ is given by the reference axes h, k as in Fig. 1.

For the elliptical curve, the following properties can be proved:

(*a*) The curve itself is symmetrical about the bisectors of the angles between $(\bar{1}11)$ and (311) or (311) and $(1\bar{1}\bar{1})$. The two bisectors are perpendicular to each other and they are a pair of similar 'planes' symmetrical about (311). The planes are imaginary because the ratios of the

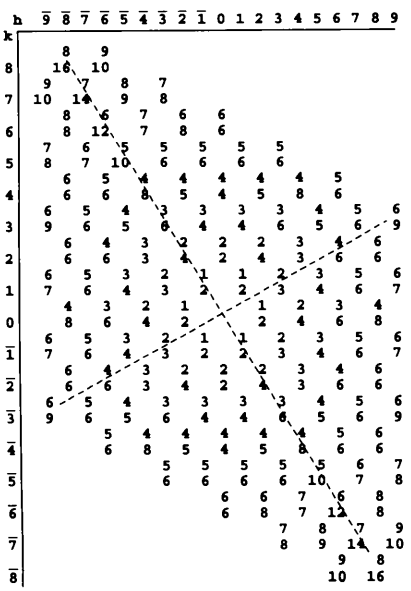

Fig. 4. The numbers of the projection of dangling bonds in the $[01\bar{1}]$ orientation within unit-length cell $D(hka)$ of a crystal surface dependent on Miller indices h, k. The oblique dashed lines mark the positions of symmetry planes $(1\bar{1}\bar{1})$ and (311).

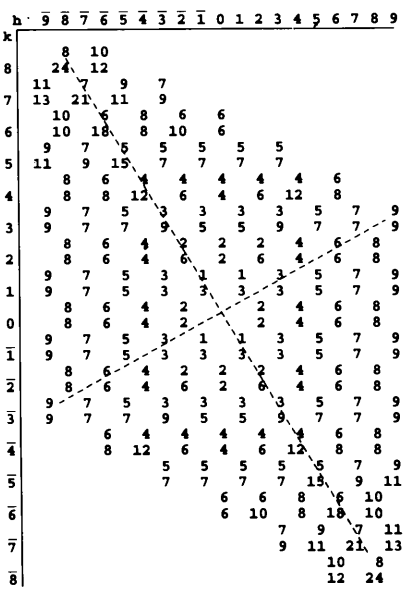

Fig. 5. Dependence of the numbers of surface dangling bonds with unit-cell area $(2^{1/2}/2)a$ on Miller indices h, k.

Miller indices h/k of the two planes are $\frac{1}{2}(-5+33^{1/2})$ and $\frac{1}{2}(-5-33^{1/2})$, respectively.

(*b*) The maximum ratio R_{max} is on the bisector of the angle between $(\bar{1}11)$ and (311) $[h/k=\frac{1}{2}(-5+33^{1/2})]$, $R_{max}=1.192$. The minimum ratio R_{min} is on the bisector of the angle included between (311) and $(1\bar{1}\bar{1})$ $[h/k=\frac{1}{2}(-5-33^{1/2})]$, $R_{min}=0.8387$. $R_{max}\times R_{min}=1$.

(*c*) The values of R for the symmetrical planes (311), $(\bar{1}11)$, $(\bar{3}\bar{1}\bar{1})$, $(1\bar{1}\bar{1})$ are unity. The values of R for the planes located between $(\bar{1}11)$ and (311) or $(1\bar{1}\bar{1})$ and $(\bar{3}\bar{1}\bar{1})$ are greater than unity. The values of R for the planes located between (311) and $(1\bar{1}\bar{1})$ or $(\bar{3}\bar{1}\bar{1})$ and $(\bar{1}11)$ are less than unity.

4. Dual epitaxy

Epitaxy is defined as the oriented crystalline growth of a material on another crystalline material. The overlayer always copies the structure and orientation of the substrate in homoepitaxy. In the case of heteroepitaxy, however, the mismatch of the lattice makes the interface incoherent. In low-mismatch heteroepitaxy, the interfacial strain is relaxed by dislocation or misorientation epitaxy. In high-mismatch heteroepitaxy, except the two ways mentioned above, the dual epitaxy will occur under suitable growth condition to relax the mismatch.

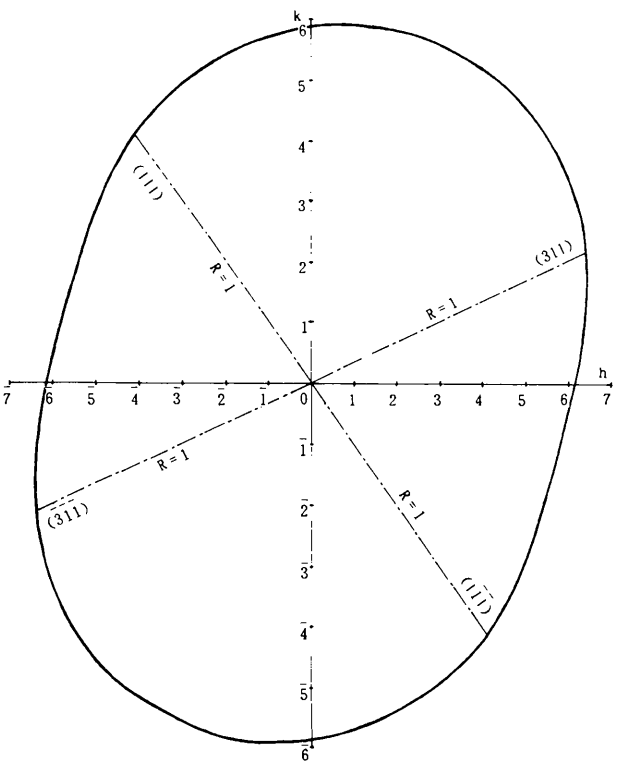

Fig. 6. Polar diagram of the ratio (R) of the unit length of surface $(h_2k_2k_2)$ to that of its similar pair $(h_1k_1k_1)$ *versus* the azimuth of plane $(h_1k_1k_1)$. The azimuth of plane $(h_1k_1k_1)$ is determined referred to axes h, k. The value of R is measured in radial dimensions. For the cases that $(h_1k_1k_1)$ is (311), $(\bar{3}\bar{1}\bar{1})$, $(1\bar{1}\bar{1})$ or $(\bar{1}11)$, $R=1$.

In dual epitaxy, the orientation of the overlayer is different from that of the substrate and is not tilted by a small angle with respect to the substrate as in the case of misorientation epitaxy. But the orientation of the overlayer is not arbitrary. Since the overlayer is single crystalline, the adoption of the orientation of the overlayer should make the interface between overlayer and substrate a step join. The symmetry of the similarity of the surface step structure in zinc blende structure makes this possible. In fact, all three kinds of dual epitaxy phenomena that have been observed so far, (111)/(100), (133)/(211), (011)/(311), occurred in accordance with the rule of the symmetry of similarity. First, the three pairs of planes are similar plane pairs. Second, as shown in the HRTEM images of the interfaces of (111)CdTe/(100)GaAs (Ponce *et al.*, 1986; Otsuka *et al.*, 1985) and (133)CdTe/(211)GaAs (Nakamura *et al.*, 1992), along the direction perpendicular to the $[01\bar{1}]$ axis the interfacial atomic structure is characterized by a unit length – by unit-length matching (*i.e.* by a step join) across the interface. Therefore, the symmetry of similarity of the surface step structure in the zinc blende structure is a basic factor in the occurrence of dual epitaxy.

It can be imagined that the dual epitaxy may occur between other similar plane pairs given by the symmetry of similarity, more precisely, given by transformation (4) or (5). The fact that the similarity of the surface step structure exists among three planes suggests that three-orientation epitaxy (not only dual epitaxy) may occur under suitable conditions.

The occurrence of dual epitaxy always contributes to the reduction of interfacial mismatch. But the reduction of mismatch is only achieved in one dimension, which is perpendicular to the $[01\bar{1}]$ axis. The interfacial mismatch on this dimension is measured by the difference of unit length $D(hka)$. When dual epitaxy occurs, the absolute value of the unit-length mismatch will certainly be lower than that of the lattice-parameter mismatch:

$$(a_1-a_2)/a_1 < [D(h_2k_2a_2)-D(h_1k_1a_1)]/D(h_1k_1a_1) < (a_2-a_1)/a_1, \quad a_2>a_1, \tag{7}$$

where 1 and 2 denote the substrate and thin-film overlayer, respectively. From the definition of $D(hka)$ given above, we obtain

$$D(h_ik_ia_i)=D(h_ik_ia)(a_i/a), \tag{8}$$

where i denotes an arbitrary crystal plane. Thus, inequality (7) can be simplified to

$$2a_1/a_2-1<\frac{D(h_2k_2a)}{D(h_1k_1a)}<1, \quad a_2>a_1. \tag{9}$$

It is evident that the ratio of the lattice parameters of the two materials conditions the orientation of the overlayer.

All of the three kinds of dual epitaxy mentioned above conform to inequality (9). For the CdTe overlayer on GaAs, $2a_{GaAs}/a_{CdTe} - 1 = 0.7446$ and $D(11a)/D(20a) = 0.8660$, $D(13a)/D(42a) = 0.8898$; $D(02a)/D(31a) = 0.8528$.

If $D(h_2k_2a_2) = D(h_1k_1a_1)$, *i.e.*

$$R = \frac{D(h_2k_2a)}{D(h_1k_1a)} = \frac{a_1}{a_2}, \quad R_{min} \le \frac{a_1}{a_2} \le R_{max}, \tag{10}$$

is satisfied, the lattice mismatch in one dimension is relaxed completely. Since the curve R in Fig. 6 is symmetrical, there are two pairs of planes that satisfy condition (10).

5. Discussion on the application of dual epitaxy

New dual epitaxy can be designed to optimize the interfacial quality in heteroepitaxy by applying the knowledge of similar plane pairs. However, some new contradictions will arise as old ones are resolved.

A. Interfacial mismatch

The reduction of interfacial mismatch is the main advantage of dual epitaxy. Thus, dual epitaxy can be utilized to reduce the interfacial mismatch. For this purpose, we can look for the optimal plane pair as the planes of the substrate and the epilayer using inequality (9), equation (10) and Fig. 6. Although (10) is the ideal condition for the reduction of mismatch, it is usually not a favourable condition for other factors that play an important role in the occurrence of dual epitaxy or the quality of the interface. In particular, for two materials for which the lattice mismatch is excessively high, *i.e.* $a_1/a_2 > 1.192$ or $a_1/a_2 < 0.8387$, (10) is in contradiction with inequality (9). Thus, we should look for the optimum pair of planes within the angle included between the two pairs of planes with $R = 1$ and $R = 2a_1/a_2 - 1$ ($R = 1.192$ when $a_1/a_2 > 1.192$; $R = 0.8387$ when $a_1/a_2 < 0.8387$), respectively, and nearer to the pair of planes with $R = a_1/a_2$ ($R = 1.192$ when $a_1/a_2 > 1.192$; $R = 0.8387$ when $a_1/a_2 < 0.8387$) in Fig. 6.

B. Interfacial net charge

For the parallel heteroepitaxy between group IV diamond structure and III–V or II–VI zinc-blende-structure materials or between III–V and II–VI zinc-blende-structure materials, the ideal planar geometry is only allowed for the nonpolar planes. In the case of polar heteroepitaxy, charge will accumulate at the interface. This is harmful to the quality of the interface. Farrell *et al.* (1991) described an approach of achieving the balance of net charge at the growth interface between II–VI and III–V materials, which is based on the design of surface reconstruction.

For the case of dual epitaxy, the balance of the net charge at the interface with ideal planar geometry can be achieved not only for the nonpolar planes but also for some polar planes.

In the case of dual epitaxy between group IV diamond-structure and III–V or II–VI zinc-blende-structure materials, since the surface of group IV materials is always nonpolar, the balance of the interfacial net charge with ideal planar geometry can be achieved only for the nonpolar planes of the zinc-blende-structure materials. As mentioned above, the planes with index $h = 4m$ (m is an integer) are nonpolar.

In the case of dual epitaxy between group III–V and II–VI zinc-blende-structure materials, the planes of the substrate and the overlayer cannot be nonpolar simultaneously because the indices h of a pair of similar planes cannot be even numbers simultaneously. However, the balance of the net charge at an interface with ideal planar geometry can be achieved for certain pairs of planes.

For diamond- and zinc-blende-structure crystals, the nonpolar surface is characterized by the fact that each dangling bond contains one electron on average. Similarly, if each dangling bond of two crystal surfaces contains one electron on average, the heteroepitaxic interface between the two crystal surfaces will achieve the balance of net charge. Let $n_{b\mathrm{III}}$, $n_{b\mathrm{V}}$, $n_{b\mathrm{II}}$ and $n_{b\mathrm{VI}}$ denote the numbers of dangling bonds of group III, V, II and VI atoms within the unit cell of the surface, respectively. Since each dangling bond of the group III, V, II or VI atom on the surface of the zinc-blende-structure crystal contains $\frac{3}{4}$, $\frac{5}{4}$, $\frac{2}{4}$ or $\frac{6}{4}$ electrons, respectively, the balance condition of the net charge at the dual epitaxic interface of group III–V and II–VI materials can be written in the form

$$\tfrac{3}{4}n_{b\mathrm{III}} + \tfrac{5}{4}n_{b\mathrm{V}} + \tfrac{2}{4}n_{b\mathrm{II}} + \tfrac{6}{4}n_{b\mathrm{VI}} = n_{b\mathrm{III}} + n_{b\mathrm{V}} + n_{b\mathrm{II}} + n_{b\mathrm{VI}}. \tag{11}$$

Remembering the definitions of 'net bond number', at the epitaxic interface,

$$\begin{aligned} n_{nb\mathrm{III-V}} &= n_{b\mathrm{III}} - n_{b\mathrm{V}}, \\ n_{nb\mathrm{VI-II}} &= n_{b\mathrm{VI}} - n_{b\mathrm{II}}, \end{aligned} \tag{12}$$

and putting (12) in (11), we obtain

$$n_{nb\mathrm{III-V}} = 2n_{nb\mathrm{VI-II}}. \tag{13}$$

Since the admissible values of n_{nb} are 0, ±1, ±2 and ±3, the solution is

$$\begin{aligned} n_{nb\mathrm{III-V}} &= \pm2, \\ n_{nb\mathrm{VI-II}} &= \pm1. \end{aligned} \tag{14}$$

Thus, the plane of group III–V material should be the one with index $h_1 = 4m_1 + 2$ (m_1 is an integer) and the plane of group II–VI material should be the one with index $h_2 = 4m_2 \pm 1$ (m_2 is an integer).

For the dual epitaxic interface between the same group zinc-blende-structure materials, remembering that there is only one plane with even Miller indices h within the three planes of a similar group, we should select odd numbers for the indices h of both substrate and overlayer.

In general, the charge density of the surface introduced by dangling bonds decreases as the Miller indices of the surface increases and thus adopting the planes with high Miller indices for epitaxy can decrease the interfacial charge density to a certain value.

C. Meeting of bonds at interface

For a pair of similar planes, equality of the number of projections of dangling bonds within unit length of the two surfaces ensures some coherency between the overlayer and substrate and thus aids the occurrence of dual epitaxy. However, the numbers of dangling bonds n_b within the unit-cell area of the two ideal surfaces are usually unequal and this is an unfavourable factor for the occurrence of dual epitaxy and the quality of the interface. However, reconstruction of the real surface of the substrate usually results in dimerization between two dangling bonds and thus reduces the number of dangling bonds on the surface. So the incident atoms can be placed in the correct positions to lead to dual epitaxy.

For this reason, dual epitaxy only occurs on certain reconstructed surfaces. Surface reconstruction plays an important role in the occurrence of dual epitaxy, as has been shown in many experiments.

As mentioned above, one of the values of n_b of a plane located between (311) and $(1\bar{1}\bar{1})$ or $(\bar{3}\bar{1}\bar{1})$ and $(\bar{1}11)$ in Fig. 1 or Fig. 6 is always greater than one of the values of n_b of its similar pair located between $(\bar{1}11)$ and (311) or $(1\bar{1}\bar{1})$ and $(\bar{3}\bar{1}\bar{1})$. Thus, within a pair of similar surfaces, the one located between (311) and $(1\bar{1}\bar{1})$ or $(\bar{3}\bar{1}\bar{1})$ and $(\bar{1}11)$ is suitable for the role of substrate in dual epitaxy. Since the ratio of the surface unit length R corresponding to each plane $(h_1k_1k_1)$ located within this zone is less than one, the dual epitaxy is more liable to occur in the case that the lattice parameter of the overlayer is longer than that of substrate. The effect of surface tension also leads to the same result.

D. Optimum surface step structure

It can be seen in Fig. 1 that, on a surface with odd Miller indices h, k, the surface atomic arrangement within any unit length has a displacement $(2^{1/2}/4)a$ in the $[01\bar{1}]$ direction from that within its adjacent unit length; the real unit length is $2D(hka)$. Thus, for the case that the Miller indices of the substrate and the epilayer are odd and even, respectively, the epitaxic growth on an ideal planar surface of the substrate will result in a twin boundary between adjacent unit lengths $[D(hka)]$. In fact, no experiment has shown such a result and real surfaces are usually non-ideally planar.

Studying Fig. 1, we find that a tooth-like interface will avoid the problem. The width of such a tooth is $2D(hka)$; the two oblique planes of each tooth are (111) or (200) planes at obtuse angles with the plane of the substrate and are terminated with anions and cations, respectively. Thus, the interfaces of different dual epitaxies will be included in the interface of (111)/(200) or the combinations of (111)/(200) and (111)/(111). In particular, at the interface between (111) and (200) planes, one oblique plane of the tooth disappears, thus the interface is a real plane. As an example, the tooth-like interfaces of $(1\bar{3}\bar{3})$, (422) and $(\bar{5}11)$ are shown in Fig. 7.

On such tooth-like surfaces, the conclusions about the symmetry of similarity of the surface step structure, the surface dangling-bond density and the surface charge density (or 'net bond' density) still hold good. Thus, such a tooth-like dual epitaxic interface can avoid all the geometrical and electrical troubles mentioned above. The remaining problem is the energy-dependent and experimental possibility of realizing such a tooth-like surface.

6. Concluding remarks

In summary, the symmetry of similarity in zinc-blende- (or diamond-) structure crystals brought about harmonious relations of surface step structure and the density and arrangement of surface dangling bonds between different planes; this is the intrinsic factor of the

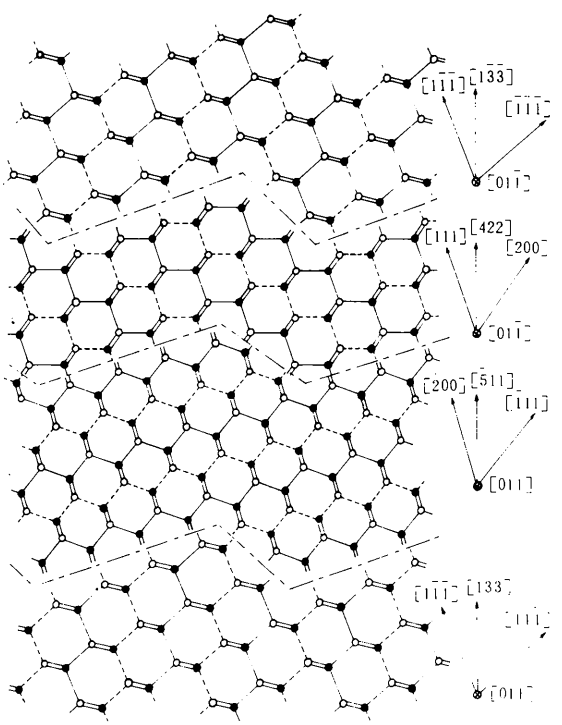

Fig. 7. The tooth-like interfaces of $(1\bar{3}\bar{3})$, $(\bar{5}11)$ and (422).

occurrence of dual epitaxy. The reduction in interfacial mismatch introduced by dual epitaxy promotes the occurrence of dual epitaxy. In dual epitaxy, the factors that impair the quality of interface and epilayer, such as interfacial mismatch, interfacial net charge and some twins, can be remitted or avoided by adopting suitable planes of substrate and epilayer and appropriate surface reconstruction. Of course, the achievement of an ideal dual epitaxy depends on growth conditions and surface reconstruction and therefore on energy in the final analysis, which includes surface energy, interfacial energy, and kinetic and thermodynamic energies.

The author sincerely thanks Dr A. Y. Cho and Mr S. D. Chen for their suggestions and Mr J. J. Yuan, Ms H. Lin, Ms F. Li, Mr J. Li and Mr Y. S. Luo for their assistance.

References

CINADER, G. & RAIZMAN, A. (1992). *J. Appl. Phys.* **71**, 2202–2205.
COHEN-SOLAR, G., BAILLY, F. & BARBE, M. (1986). *Appl. Phys. Lett.* **49**, 1519–1521.
FARRELL, H. H., TAMARGO, M. C., DE MIGUEL, J. L., TURCO, F. S., HWANG, D. M. & NAHORY, R. E. (1991). *J. Appl. Phys.* **69**, 7021–7028.
FELDMAN, R. D. & AUSTIN, R. F. (1986). *Appl. Phys. Lett.* **49**, 954–956.
LANGE, M. D., SPORKEN, R., MAHAVADI, K. K., FAURIE, J. P., NAKAMURA, Y. & OTSUKA, N. (1991). *Appl. Phys. Lett.* **58**, 1988–1990.
NAKAMURA, Y., OTSUKA, N., LANGE, M. D., SPORKER, R. & FAURIE, J. P. (1992). *Appl. Phys. Lett.* **60**, 1372–1374.
NISHITANI, K., OHKATA, R. & MUROTANI, T. (1983). *J. Electron Mater.* **12**, 619–635.
ORTNER, B. & BAUER, G. (1988). *J. Cryst. Growth*, **92**, 69–76.
OTSUKA, N., KOLODZIEJSKI, L. A., GUNSHOR, R. L., DATTA, S., BICKNELL, R. N. & SCHETZINA, J. F. (1985). *Appl. Phys. Lett.* **46**, 860–862.
PONCE, F. A., ANDERSON, G. B. & BALLINGALL, J. M. (1986). *Surf. Sci.* **168**, 564–570.
SMITH, L. M., BYRNE, C. F., PATEL, D., KNOWLES, P. & THOMPSON, J. (1990). *J. Vac. Sci. Technol.* A**8**, 1078–1085.

Acta Cryst. (1995). A**51**, 909–916

Crystal Space Analysis by means of Voronoi–Dirichlet Polyhedra

BY V. A. BLATOV, A. P. SHEVCHENKO AND V. N. SEREZHKIN

Samara State University, Ac. Pavlov St. 1, 443011 *Samara, Russia*

(*Received* 20 *January* 1995; *accepted* 22 *May* 1995)

Abstract

The method of analysis of crystal space topology by means of Voronoi–Dirichlet tessellation is described. The possibilities of using Voronoi–Dirichlet polyhedra in the investigation of local and global geometrical/topological properties of the crystal lattice in structures of simple and complex substances are discussed. Examples of the application of the proposed method in crystal-chemical analysis are given.

1. Introduction

At present, geometrical analysis of crystal structure is one of the fundamental methods that are used by crystal chemists in solid-state investigation. Within this approach, the continuous crystal space is replaced by the discrete (pointal) space, and geometrical properties of a set of points, symbolizing centres of gravity of maxima of electron density or structural units (atoms or atomic groups), are analysed. This set, otherwise known as the multiregular system (MRS), is a set of N regular systems of points (where N is a number of crystallographically independent structural units) and a special type of Delauney system (Galiulin, 1984). The crystal space is usually considered as space $\mathbf{R}^3$ in which the MRS is embedded (space $\mathbf{M}^3$), or as space $\mathbf{M}^3$ in each point of which the function of electronic density $\rho(\mathbf{x}, \mathbf{y}, \mathbf{z})$ is determined, and positive integer $\mathbf{Z}_i$, which is equal to the charge of a corresponding atom, is compared with each point $\mathbf{p}_i$ of the MRS (space $\mathbf{P}^3$).

According to numerous investigations, the geometrical/topological properties of a MRS are connected with the energy characteristics of a crystal. In crystal chemistry analysis, however, very little attention is paid to topological properties of a MRS and $\mathbf{M}^3$ as a rule. Although such terms as 'topology of a coordination polyhedron' or 'topology of a complex group' are commonly used, they do not usually assume the performance of a comprehensive analysis of topological properties of the discussed objects. A theoretical foundation for the topological part of geometrical crystallography has been carried out by a number of authors (particularly Galiulin, 1984; Wells, 1977; Pearson, 1972; Engel, 1986), but the methods of mathematical analysis of $\mathbf{M}^3$ topology features are far